


RESEARCH ARTICLE OPEN ACCESS

Divergent Biochemical Properties and Disparate Impact of Arrhythmogenic Calmodulin Mutations on Zebrafish Cardiac Function

Sahar I. Da'as^{1,2} | Angelos Thanassoulas³ | Brian L. Calver⁴ | Alaaeldin Saleh³ | Doua Abdelrahman¹ | Waseem Hasan¹ | Bared Safieh-Garabedian³ | Iris Kontogianni^{5,6} | Gheyath K. Nasrallah^{7,8} | George Nounesis⁵ | F. Anthony Lai^{3,4} | Michail Nomikos³ 

¹Department of Human Genetics, Sidra Medicine, Doha, Qatar | ²College of Health and Life Sciences, Hamad Bin Khalifa University, Doha, Qatar | ³College of Medicine, QU Health, Qatar University, Doha, Qatar | ⁴Sir Geraint Evans Wales Heart Research Institute, College of Biomedical and Life Science, Cardiff University, Cardiff, UK | ⁵National Centre for Scientific Research "Demokritos", Agia Paraskevi, Greece | ⁶National Technical University of Athens, Athens, Greece | ⁷Biomedical Research Center, Qatar University, Doha, Qatar | ⁸Department of Biological Sciences, College of Health Sciences, QU Health, Qatar University, Doha, Qatar

Correspondence: Michail Nomikos (mnomikos@qu.edu.qa)

Received: 28 December 2023 | **Revised:** 4 June 2024 | **Accepted:** 12 June 2024

Funding: Qatar Foundation, Grant/Award Numbers: HSREP02-1125-190004, UREP26-097-3-040; Qatar University, Grant/Award Numbers: QUCG-CMED-19/20-2, QUCG-CMED-22/23-514

Keywords: arrhythmias | calcium | calmodulin | cardiac disease | zebrafish

ABSTRACT

Calmodulin (CaM) is a ubiquitous, small cytosolic calcium (Ca²⁺)-binding sensor that plays a vital role in many cellular processes by binding and regulating the activity of over 300 protein targets. In cardiac muscle, CaM modulates directly or indirectly the activity of several proteins that play a key role in excitation-contraction coupling (ECC), such as ryanodine receptor type 2 (RyR2), L-type Ca²⁺ (Ca_v1.2), sodium (NaV1.5) and potassium (KV7.1) channels. Many recent clinical and genetic studies have reported a series of CaM mutations in patients with life-threatening arrhythmogenic syndromes, such as long QT syndrome (LQTS) and catecholaminergic polymorphic ventricular tachycardia (CPVT). We recently showed that four arrhythmogenic CaM mutations (N98I, D132E, D134H, and Q136P) significantly reduce the binding of CaM to RyR2. Herein, we investigate in vivo functional effects of these CaM mutations on the normal zebrafish embryonic heart function by microinjecting complementary RNA corresponding to CaM^{N98I}, CaM^{D132E}, CaM^{D134H}, and CaM^{Q136P} mutants. Expression of CaM^{D132E} and CaM^{D134H} mutants results in significant reduction of the zebrafish heart rate, mimicking a severe form of human bradycardia, whereas expression of CaM^{Q136P} results in an increased heart rate mimicking human ventricular tachycardia. Moreover, analysis of cardiac ventricular rhythm revealed that the CaM^{D132E} and CaM^{N98I} zebrafish groups display an irregular pattern of heart beating and increased amplitude in comparison to the control groups. Furthermore, circular dichroism spectroscopy experiments using recombinant CaM proteins reveals a decreased structural stability of the four mutants compared to the wild-type CaM protein in the presence of Ca²⁺. Finally, Ca²⁺-binding studies indicates that all CaM mutations display reduced CaM Ca²⁺-binding affinities, with CaM^{D132E} exhibiting the most prominent change. Our data suggest that CaM mutations can trigger different arrhythmogenic phenotypes through multiple and complex molecular mechanisms.

Sahar I. Da'as and Angelos Thanassoulas contributed equally to this study.

This is an open access article under the terms of the [Creative Commons Attribution](https://creativecommons.org/licenses/by/4.0/) License, which permits use, distribution and reproduction in any medium, provided the original work is properly cited.

© 2024 The Author(s). *Journal of Cellular Biochemistry* published by Wiley Periodicals LLC.

1 | Introduction

Calmodulin (CaM) is a small, ubiquitously expressed Ca^{2+} -binding protein, which consists of 148 amino acids and has a molecular weight of 16.7 kDa. Regardless of its small size, CaM plays an essential role in many cellular processes by binding and regulating the activity of over 300 protein partners [1–4]. CaM's ability to interact with such a wide range of different proteins is attributed to its structural plasticity. Structurally, CaM is composed of an N- and a C-terminal lobe, which are connected by a flexible linker. Each lobe contains two Ca^{2+} -binding EF-hand domains. EF hands I and II are located at the N-terminal and EF hands III and IV at the C-terminal lobe. Ca^{2+} binding to CaM leads to conformational changes that expose the hydrophobic surfaces within the N- and C-lobes of CaM, enabling them to interact with the target proteins [5]. Interestingly, the C-terminal lobe of CaM has a sixfold higher affinity ($K_d = 2.5 \mu\text{M}$) for Ca^{2+} compared to the N-terminal lobe ($K_d = 16 \mu\text{M}$) [6]. CaM is also a unique example of evolutionary conservation and genetic redundancy. It shows 100% protein sequence identity among vertebrates and is encoded by three nonallelic CaM genes (*CALM1*, *CALM2*, and *CALM3*), which are located at human chromosomes 14q24-q31, 2p21.1-p21.3, and 19q13.2-q13.3, respectively [7, 8]. Interestingly, over the last decade more than 30 missense mutations in CaM genes have been identified and directly linked with congenital arrhythmogenic cardiac disorders displaying a broad spectrum of clinical presentations, including catecholaminergic polymorphic ventricular tachycardia (CPVT), long QT syndrome (LQTS) and idiopathic ventricular fibrillation (IVF) [1, 9–14].

Due to the complex multifunctional role of CaM within the cardiomyocytes, multiple molecular mechanisms have been proposed through which CaM missense mutations may lead to severe arrhythmogenic cardiac disease. One of the primary mechanisms involves abnormal levels of cytosolic Ca^{2+} concentration resulting from either abnormal Ca^{2+} entry through defective inactivation of L-type Ca^{2+} channels ($\text{Ca}_v1.2$), or from increased sarcoplasmic reticulum (SR) Ca^{2+} “leakage” due to diminished inhibition of cardiac ryanodine receptor 2 (RyR2) [15–20]. It has been well established that CaM binds to, and lowers the open probability of, RyR2 at both low and high cytosolic Ca^{2+} concentrations. This CaM regulation of RyR2 channel activity is vital for normal cardiac function as aberrant CaM–RyR2 interaction has been reported to result in life-threatening cardiovascular dysfunction [21–23]. Moreover, multiple studies have shown that a number of the reported CaM mutations result in a defective CaM–RyR2 binding and thus inhibition, which may result in delayed afterdepolarizations [15, 16, 18, 20, 24, 25].

We recently showed that four de novo missense mutations in *CALM2* gene, identified in two patients presenting with LQTS (p.N98I, p.D134H) and two with clinical features of both LQTS and CPVT (p.D132E and p.Q136P), lead to considerable reduction of CaM–RyR2 interaction and defective modulation of [^3H]ryanodine binding to RyR2 due to disparate binding properties of CaM mutants with two RyR2 regions (3581–3607aa and 4255–4271aa), which contribute to a previously proposed RyR2-binding pocket [25–27].

In the present study, we applied a multidisciplinary approach to further characterize and understand the molecular mechanisms utilized by these pathogenic *CALM2* mutations (p.N98I, p.D132E, p.D134H, and p.Q136P), that lead to different clinical presentations of severe arrhythmogenic cardiac disease. The in vivo validation employed the powerful zebrafish model, as we have previously demonstrated using CaM^{E105A} [24]. Synthetic complementary RNA (cRNA) encoding the CaM^{N98I}, CaM^{D132E}, CaM^{D134H}, and CaM^{Q136P} mutants was individually micro-injected into zebrafish embryos and the effects of expressing these CaM mutations in embryonic heart upon normal cardiac function were investigated. In addition, we bacterially expressed and affinity-purified the four CaM mutants to investigate the impact of these mutations on the biophysical and biochemical properties of each recombinant CaM protein. More specifically, we used circular dichroism (CD) spectroscopy to compare the thermal and chemical stabilities of the wild-type and mutant CaMs, in the presence and absence of Ca^{2+} . Moreover, the Ca^{2+} binding affinities of both N- and C-lobes of CaM wild-type and mutants were estimated and directly compared by monitoring the intrinsic tyrosine and phenylalanine fluorescence, respectively.

2 | Materials and Methods

2.1 | Plasmid Construction

Human CaM (GenBank accession number AAD45181.1) in pHSIE plasmid [18, 20] was subjected to site-directed mutagenesis (QuikChange II; Stratagene) to generate the four CaM mutant constructs. Successful mutagenesis was confirmed by dideoxynucleotide sequencing (Applied Biosystems Big-Dye Ver 3.1 chemistry and model 3730 automated capillary DNA sequencer by DNA Sequencing & Services). CaM^{WT} and CaM mutant constructs were then amplified by polymerase chain reaction (PCR) from pHSIE plasmid using Phusion polymerase (Thermo Fisher Scientific) and the appropriate primers to incorporate 5'-KpnI and 3'-NotI sites and then cloned into the pCDNA3.1(+) expression vector. The primers used for the amplification of the CaM constructs were: 5'-GGAAGGTACCATGGCTGATCAGCTGACCGAAG-3' (forward) and 5'-GCAAGCGCCGCTCATTTTGCAGTCATCATC TGTAC-3' (reverse).

2.2 | Zebrafish Care and Husbandry

Zebrafish (*Danio rerio*) wild-type line (AB strain) adults were maintained in a recirculating aquaculture system under standard environmental conditions of temperature at 27–28°C, conductivity at 800 μS , and pH at 7.5 with 14 h light and 10 h dark cycle. All protocols used in these studies were approved by the local Animal Care and Use Committee, and conformed to the Zebrafish Policy published by the Qatar Ministry of Public Health following the Guide for the Care and Use of Laboratory Animals published by the National Institutes of Health. Experiments performed on zebrafish followed Qatar Foundation, IACUC Office approval (Protocol Number: EVMC-2020-006). For the cRNA injection experiments, embryos were collected in

N-phenylthiourea (PTU) media, used for microinjection, and raised in a 28°C incubator. Larvae at 72 h postfertilization (hpf) were used for phenotypic examination and imaging of cardiac function analysis, as previously described [24]. Zebrafish larvae were euthanized by administration of an overdose of Tricaine MS-222 anesthetic agent (200 mg/L) followed by chilling on ice. Upon euthanasia, zebrafish carcasses were disposed of as medical waste.

2.3 | cRNA Synthesis and Zebrafish Embryos Microinjection

Calmodulin constructs (CaM^{WT} and CaM^{variants}) were linearized and the respective CaM cRNA was synthesized by the mMessage Machine T7 kit (Thermo Fisher Scientific) and then was polyadenylated using the poly(A) tailing kit (Thermo Fisher Scientific), as per manufacturer's instructions. Zebrafish embryos were injected at 1–2 cell stages with approximately 2 nL of 150 ng/μL cRNA under Zeiss Stemi 2000-C stereomicroscope. The zebrafish CaM^{WT}, CaM^{variants}, and control (uninjected) were examined for the cardiac phenotype. At least 50 embryos were injected per each group for three sets of experiments.

Comparable CaM^{WT} and CaM^{variants} protein expression in the zebrafish embryos was confirmed by western blot analysis using an anti-CALM1 antibody (1:5000 dilution; Source Bioscience), as previously described [24].

2.4 | Gross Examination of Zebrafish Groups

The survival rates of the different zebrafish groups were assessed at 24 hpf. The zebrafish development classification was carried out at 72 hpf, before imaging. The cardiac phenotypes were examined by video recordings at 72 hpf using a Stereomicroscope Zeiss LUMAR.V12 with Plan Apo S ×1.5 objective. Cardiac function was assessed using Micro-Manager and ImageJ (BSD-2). Time-lapse videos were captured at 60 frames per second (fps) at a magnification of ×150 using a monochrome camera (The Imaging Source, model DMK 33UX252) at 1920 × 1080 resolution. The examined zebrafish groups were sorted into an individual well in a 28°C incubator and removed from the incubator just before imaging. To minimize the environmental temperature impact on cardiac function, zebrafish larvae were mounted for stabilization in 2.5% methylcellulose (Sigma, Cat# M0387), before imaging under the stereomicroscope equipped with a heated glass stage at 28°C. The zebrafish in different groups were examined for developmental or teratogenic defects, and if they had any, these larvae were excluded from the cardiac analysis. Cardiac functions of heart rate and cardiac activity were analyzed by DanioScope software (video-based analysis tool) (Noldus, the Netherlands).

2.5 | Analysis of Heart Rhythm and Heart Rate

To analyze the functional impact of the human genetic variants, recorded videos of zebrafish at 72 hpf were imported

into the DanioScope software (Noldus, version 1.0.109) as uncompressed AVI files, where subsets of the beating heart chambers were outlined. The heart rate was calculated from 60 fps video recordings of the heart area. For the inter-beat interval analysis, DanioScope software analyzes dynamic pixel changes in grayscale values on a per-pixel basis within specified regions of interest. These areas of interest are drawn to include the cardiac chambers that are actively contracting in the heart of lateral-positioned larvae. The software automatically calculated the inter-beat interval and the average percentage of pixels that show changes in grayscale values compared to the previous frame over the time using the raw data (diastole-systole conditions).

2.6 | Protein Expression and Purification

For protein expression, *Escherichia coli* (BL21-CodonPlus (DE3); ThermoFisher) cells were transformed with the appropriate pHSIE-CaM plasmid, and cultured at 37°C until the OD₆₀₀ nm reached 0.6. After optimization experiments, protein expression was induced for 18 h at 16°C with 0.1 mM IPTG (isopropyl β-D-thiogalactopyranoside) (Sigma-Aldrich). The bacterial cell pellets were harvested by centrifugation at 6000g for 15 min at 4°C. Recombinant CaM proteins were then purified as previously described [20, 25].

2.7 | CD Spectroscopy; Thermal and Chemical Stability Analysis

Folding and stability of CaM^{WT} and its corresponding mutants were assessed by CD spectroscopy. Spectra, melting curves, and chemical stability measurements were recorded on an Aviv 215 instrument (Aviv Biomedical Inc., Lakewood, NJ) equipped with a thermostatted cell holder using 0.1-cm quartz cuvettes. Proteins ($c = 6\text{--}8\ \mu\text{M}$) were dissolved in 100 mM KCl, 10 mM 4-(2-hydroxyethyl)-1-piperazineethanesulfonic acid (HEPES), pH 7.4, including either 1 mM CaCl₂ or 1 mM ethylenediaminetetraacetic acid. Concentrations were determined by absorption spectroscopy using $\epsilon_{230\text{ nm}} = 41,250\ \text{M}^{-1}\ \text{cm}^{-1}$ [28]. Melting curves were recorded at 221 nm in 0.5°C intervals with parameters resulting in a temperature gradient of ca. 30°C/h.

Chemical stability was measured by mixing the samples with a pH-adjusted 8 M guanidinium chloride (GuHCl) stock solution including buffer and salt, and incubated overnight at room temperature. Measurements were performed at 221 nm and 25°C in ca. 0.2 M GuHCl intervals from 0 to 5 M. GuHCl concentrations including protein were determined by refractometry [29] using an Abbe-type digital refractometer (PA202, Misco, Cleveland, OH). Data were fitted assuming a 2- or a 3-state transition of the form $n \rightarrow i$ and $n \rightarrow i \rightarrow u$, respectively:

$$\Delta\epsilon(c_d) = \frac{I_n + S_n c_d + (I_u + S_u c_d) \times \exp\left[m\left(\frac{c_d - D_{50}}{RT}\right)\right]}{1 + \exp\left[m\left(\frac{c_d - D_{50}}{RT}\right)\right]}, \quad (1)$$

$$\begin{aligned} \Delta\varepsilon(c_d) &= \frac{I_n + S_n c_d + (I_i + S_i c_d) \times \exp\left(\frac{m_1(c_d - D_{50,1})}{RT}\right) + (I_u + S_u c_d) \times \exp\left(\frac{m_1(c_d - D_{50,1}) + m_2(c_d - D_{50,2})}{RT}\right)}{1 + \exp\left(\frac{m_1(c_d - D_{50,1})}{RT}\right) + \exp\left(\frac{m_1(c_d - D_{50,1}) + m_2(c_d - D_{50,2})}{RT}\right)}, \end{aligned} \quad (2)$$

where c_d represents the denaturant concentration, D_{50} the denaturant concentrations at the midpoint of the transitions, and m is a measure of the dependence of ΔG on the GuHCl concentration. The free energy change between the protein states was calculated from $\Delta G = m \cdot D_{50}$. As small concentrations of GuHCl stabilize CaM due to its ionic nature [30, 31] data obtained at 0 and 0.2 M GuHCl were excluded from fitting.

2.8 | Steady-State Fluorescent Intensity Measurements

Fluorescence measurements were made at room temperature using a Quantamaster-400 fluorometer (Photon Technology International, Inc.) equipped with a 75 W xenon short arc lamp (Ushio). All samples were dialyzed against a calcium buffering system consisting of 50 mM HEPES (pH 7.4), 100 mM KCl, 0.05 mM ethylene glycol-bis(β -aminoethyl ether)- N,N,N',N' -tetraacetic acid, and 5 mM NTA to minimize the effect of small protein concentration differences among samples.

Fluorescence emission spectra were collected from samples containing 6 μ M of protein and 4 nM of the Fluo-5N calcium indicator at various calcium concentrations ($[Total Ca^{2+}] = 0-15$ mM) using a 0.5 nm wavelength step size and 5 nm band passes. Binding to CaM N-domain binding sites was monitored using 250 nm excitation and recording phenylalanine fluorescence emission changes at 280 nm, while binding to CaM C-domain binding sites was monitored using 277 nm excitation and recording tyrosine fluorescence emission changes at 320 nm. The free calcium concentration ($[Free Ca^{2+}]$) of each sample was determined using 467 nm excitation and tracking Fluo-5N fluorescence emission changes at 510 nm. These changes can then be used to calculate $[Free Ca^{2+}]$ from the equation:

$$[Free Ca^{2+}] = K_d \frac{F^{Max} - F}{F - F^{Min}},$$

where F^{Min} and F^{Max} is the fluorescence intensity in the absence and excess (full saturation) of calcium, respectively, and F is the intensity of the sample. The dissociation constant K_d of Fluo-5N was found to be 92 ± 3 μ M in the buffer used in this study, determined in a separate experiment. All spectra were corrected by subtracting their corresponding buffer blanks and all experiments were repeated at least four times.

The resulting normalized fluorescence intensity versus $[Free Ca^{2+}]$ data were plotted and fitted to a model-independent two-site Adair function which allowed nonequal intrinsic affinities and cooperativity of the two binding sites:

$$Y = \frac{K_1 [Free Ca^{2+}] + 2K_2 [Free Ca^{2+}]^2}{2(1 + K_1 [Free Ca^{2+}] + K_2 [Free Ca^{2+}]^2)},$$

where $K_1 = k_1 + k_2$ is the sum of the intrinsic microscopic equilibrium constants of each binding site, $K_2 = k_1 k_2 k_c$ is the equilibrium constant for binding to both sites and Y is the fractional occupancy of the binding sites [32].

The intradomain cooperativity constant k_c cannot be determined analytically from these data alone, however a lower limit can be estimated from the apparent cooperativity constant K_c using following equation [33, 34]:

$$k_c^{min} = K_c = \frac{4K_2}{K_1}.$$

The apparent dissociation constants are reported as the average value for the pair of sites derived from the square root of $1/K_2$. Gibbs free energy changes (ΔG_i) were calculated using the well-known equation:

$$\Delta G_i = -RT \ln K_i,$$

where K_i is the appropriate equilibrium constant.

2.9 | Generation of Model Structures for CaM Mutants

Molecular operating environment software (MOE version 2022.02—Molecular Operating Environment [MOE], 2022.02 Chemical Computing Group ULC, Montreal, Canada) was used for the creation, visualization, representation, and analysis of the protein models. The crystal structure of calcium-bound Calmodulin (PDB ID: 1c1l) was used as the initial template. The mutations were introduced using the Protein Builder tool of the software. Missing hydrogen atoms were added using the Protonate 3D utility of MOE using the AMBER10:EHT force-field. The resulting structures were further optimized by energy minimization with the AMBER10:EHT force-field, using a 0.1 kcal/mol/ \AA^2 RMS gradient. The final structures were then superposed with the Align/Superpose tool of MOE.

3 | Results

3.1 | Expression of Arrhythmogenic CaM Mutants in Zebrafish Embryos Leads to Disparate Embryonic Heart Function Alterations

To investigate the potential in vivo effects of the four arrhythmia-associated CaM mutants, we used the zebrafish model, as we have previously successfully employed [24, 35–37]. During the last decades and since zebrafish was introduced as a model organism in research, it has been proven a very powerful tool in cardiovascular research. Its transparent nature at early stages allows the direct visualization of zebrafish internal organs [38]. In addition, due to its small size, zebrafish can survive for several days without a functioning cardiovascular

system as sufficient perfusion with oxygen can be achieved by passive diffusion [38, 39]. This gives a significant advantage compared to other vertebrate model organisms to study the heart function and cardiac defects in early heart development that would be lethal in other vertebrate organisms.

To analyze the effects of expression of four pathogenic CaM mutants on zebrafish cardiac function, cRNA corresponding to these mutants was synthesized and microinjected in parallel with CaM^{WT} cRNA into single-cell stage zebrafish embryo groups (Figure 1, upper panel). To eliminate any teratogenic or other developmental defects, gross morphology assessment was performed at 72 hpf. The groups were sorted according to development (G1: severely affected development, G2: mildly affected development, and G3: normal development). Larvae scored at G3 were only included for imaging, and larvae with severe and nonspecific edema (G1 and G2) were excluded from further analysis (Supporting Information S1: Figure 1). cRNA concentrations were titrated and comparable expression was confirmed by western blot analysis using an anti-CaM antibody (Supporting Information S1: Figure 2), as previously described [24]. The survival rate of embryos depends on the quality of eggs and fertilized embryos that alters from batch to batch or can be directly associated with the effect of the injected synthetic cRNA. In contrast to the control (uninjected) and CaM^{WT}-injected zebrafish embryo groups that showed a

survival rate of 88% and 95%, respectively, microinjection of cRNA corresponding to the four human CaM mutants appeared to have a negative effect on the survival rate of the zebrafish embryos, calculated at 24 hpf, reducing it to 66%, 79%, 78% and 71% for CaM^{N98I}, CaM^{D132E}, CaM^{D134H}, and CaM^{Q136P}-injected zebrafish embryo groups, respectively; chi-square test for trend ($p = 0.0003$) (Figure 1, lower panel). Furthermore, the different zebrafish groups were carefully examined for developmental defects and if any detected, these larvae were excluded from cardiac function analysis.

Structural examination of the zebrafish cardiac chambers to characterize the specific cardiac phenotypes following microinjection of cRNA for the human wild-type CaM and CaM mutant constructs was performed at 72 hpf. The zebrafish heart is composed of two chambers and our imaging was performed by positioning the larvae on the lateral side to visualize the ventricle, as we have previously described [37]. Analysis was performed using Danioscope software by drawing a square to capture pixel changes at the lower ventricular chamber and not at the ventricle area closer to the atrium (Supporting Information S1: Figure 3). The measured irregular beats were either too slow (bradycardia) or too fast (tachycardia). The zebrafish groups bright-field images of the ventricular chamber at diastole and systole cycles were captured (Figure 2). Examination of the heart ventricle chamber structure (traced with black dots line) at both systolic and diastolic stages revealed a negative effect in CaM^{N98I}- and CaM^{D134H}-injected groups (χ^2 test for trend, $p < 0.0001$) when compared to the control and other CaM-injected zebrafish embryo groups (Figure 2). The structural abnormalities scoring combined thickened ventricle, heart looping, and enlarged pericardial area at a percentage of 70%, 79%, 54%, and 89% for CaM^{N98I}, CaM^{D132E}, CaM^{D134H}, and CaM^{Q136P}-injected zebrafish embryo groups, respectively (Supporting Information S1: Figure 4; Figure 2 and cardiac videos).

The average heart rate was calculated for the examined zebrafish groups. When compared to the control group, which showed 150.9 beats per minute (bpm), the groups expressing the CaM^{N98I}, CaM^{D132E}, CaM^{D134H}, and CaM^{Q136P} mutants showed alterations in the zebrafish heart rate of 139.4, 119.8, 136.0, and 157.4 bpm, respectively. Expression of CaM^{D132E} and CaM^{D134H} variants resulted in a significant reduction of the zebrafish heart rate, mimicking a severe form of human bradycardia, while expression of CaM^{Q136P} resulted in an increased heart rate at 157.4 bpm, mimicking human ventricular tachycardia when compared to control zebrafish group heart rates (Figure 3). Moreover, the calculated ejection fraction (EF) percentages (%) presented similar trends that associated with low or high heart rate. Analysis of the EF demonstrated a trend that is associated with the heart rate of the corresponding variant. CaM^{N98I}, CaM^{D132E}, and CaM^{D134H} variants resulted in higher EFs of 49.7%, 51.4%, and 54.1%, respectively, while CaM^{Q136P} had lower EF at 44.7% when compared to control (uninjected) and CaM^{WT}-injected groups (46.1% and 47.9%, respectively), (Supporting Information S1: Figure 5). Although the EF% alterations were not significant, it established a trend in variability that associated with the corresponding heart rate of CaM mutants calculated at 72 hpf, might suggesting that alterations in EF% may lead to heart failure at later stages of development.

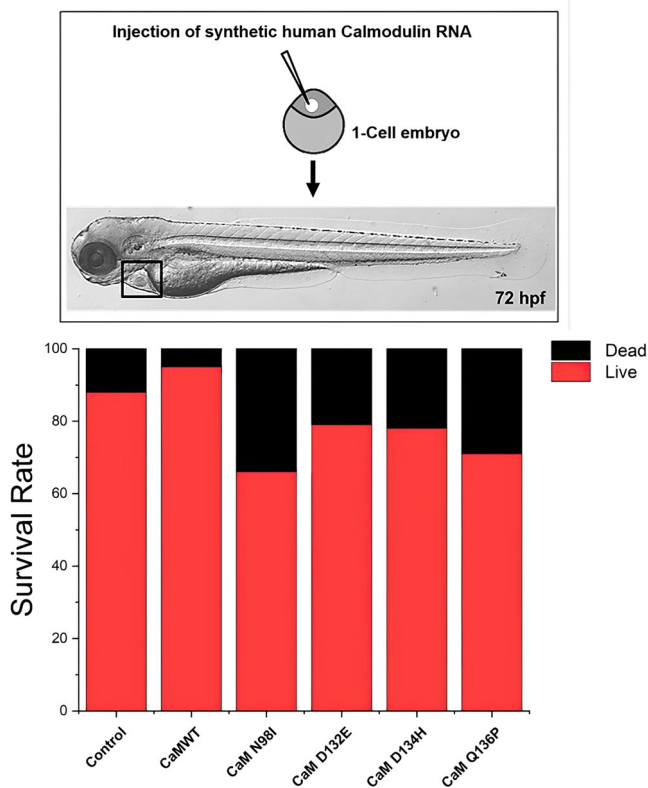


FIGURE 1 | Microinjection of human CaM cRNA variants. Representative scheme for the functional validation of the human CaM cRNA. Injection of cRNA is performed at one-cell stage embryo then the zebrafish embryos were examined for the cardiac function at 72 h postfertilization (hpf). Effect of microinjection of human CaM cRNA variants on zebrafish embryo survival (24 h) compared to Control and CaM^{WT}-injected groups, a total of three sets of experiments.

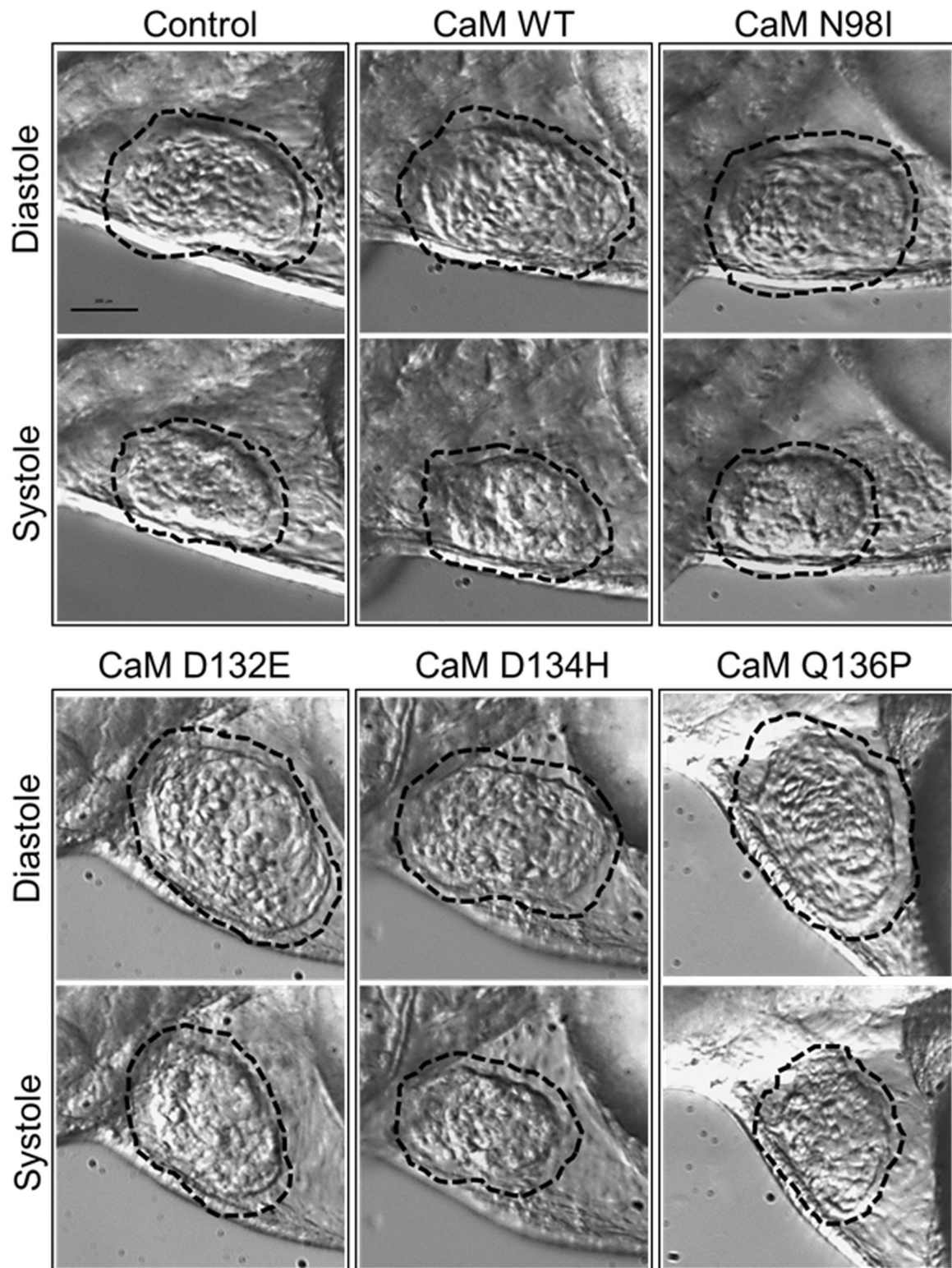


FIGURE 2 | Effect of expression of CaM variants on specific cardiac morphology in zebrafish embryos. Representative heart images at 72 h postfertilization (hpf) showing the two chambered heart (black square), image at $\times 32$. The zebrafish larvae is positioned in a lateral position and bright-field images of the ventricular chamber at diastole and systole cycles are shown. Zebrafish examined groups exhibit a well-developed ventricle, while examination of the heart ventricle chamber (traced with black dots line) at both systolic and diastolic activity showed that CaM^{D134H} and CaM^{N98I} mutant injections resulted in structural ventricle chamber abnormality when compared to the control and other CaM-injected zebrafish embryo groups.

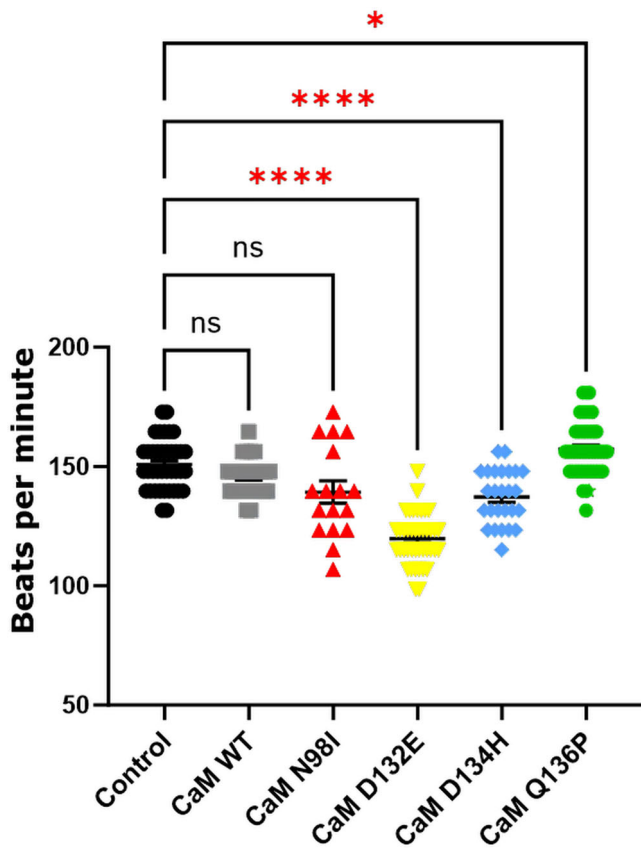


FIGURE 3 | Effect of expression of CaM variants on heart rate in zebrafish embryos. Heart rate was analyzed using Danioscope software of captured videos from zebrafish larvae at 3 days old. Microinjection of cRNA corresponding to CaM variants resulted in a decreased heart rate except CaM^{Q136P} that resulted in increased heart rate. Multiple comparisons against the control group and CaM^{WT} were performed with a one-way ANOVA test with Brown-Forsythe and Welch tests for multiple comparison using GraphPad Prism (version 9.1.1). The level of significance for the differences between groups was expressed using *p* values (**p* < 0.05 and *****p* < 0.0001 represented statistical significance) (*n* = 38, 28, 17, 41, 26 and 47 for control, CaM^{WT}, CaM^{N98I}, CaM^{D132E}, CaM^{D134H}, and CaM^{Q136P}, respectively).

Furthermore, assessment of the cardiac ventricular rhythm by analyzing the ventricular chamber activity percentage of pixel changes between diastole and systole conditions was performed. The cardiac activity signal distributed over frequencies varies according to the contraction and dilation of the heart chamber across each cardiac cycle. CaM^{D132E} and CaM^{N98I} zebrafish groups displayed an irregular pattern of heart beating in comparison to the cardiac activity percentage mean of the control, CaM^{WT}, CaM^{D134H}, and CaM^{Q136P} groups demonstrated by mean interbeat intervals (time interval between individual beats) began to elongate through the 6 s recording (Figure 4). Both CaM^{D132E} and CaM^{N98I} human mutants collectively resulted in an increased arrhythmic potential in the zebrafish model. Interestingly, the cardiac activity chart showed that CaM^{D132E} mutant amplitude fluctuates with higher extremes, and the dominant rate seems to be slower than the controls or any other cardiac activity measured for the other CaM mutants.

3.2 | Differential Impact of Arrhythmogenic Mutations on CaM Structural Stability in the Presence and Absence of Ca²⁺

To understand the divergent effects of N98I, D132E, D134H, and Q136P mutations in zebrafish cardiac function and to investigate the impact of these mutations on the biophysical and biochemical properties of wild-type CaM protein, we initially subcloned these mutants into the pHSIE plasmid expression vector. We then expressed and purified the corresponding recombinant proteins using a one-step purification protocol, as previously described [25].

Previous studies have reported the far-UV spectra of CaM^{N98I} [40], CaM^{D132E} [41], and CaMQ^{136P} [42], as well as the thermal unfolding profile of CaM^{N98I} mutant [40]. However, there is currently no study that has directly compared the far-UV CD spectra and thermal unfolding profiles of the CaM^{N98I}, CaM^{D132E}, CaM^{D134H}, and CaM^{Q136P} mutants under the same experimental conditions.

To investigate the conformations of these CaM mutants at different solvent conditions, the far-UV CD spectra of wild-type and mutant CaM proteins were recorded at both low and high temperatures in the presence and absence of Ca²⁺ (Figure 5). At 4°C, the far-UV spectra were similar, revealing a protein of high helical content, with characteristic negative peaks at 208 and 222 nm. When heated at high temperatures (≥90°C), the protein appeared to lose most of its helicity adopting a conformation closer to that of a random coil. This thermal transition is reversible and upon cooling at 4°C, the protein returns to the initial conformation. Interestingly, in the presence of Ca²⁺ some structural differences can be observed for the mutant CaM proteins at 4°C, as compared to CaM^{WT} structure, but all samples adopt the same final structure when heated at 99°C (Figure 5, lower panel). This is suggestive a different initial conformation for the mutant CaM proteins as a direct result of the various amino acid substitutions near the Ca²⁺ binding sites of the CaM molecule. This is in good agreement with previous CD studies of CaM wild-type and corresponding mutants [31, 42, 43].

The relative stability of the native CaM^{WT} and CaM mutant conformations can be assessed by thermal and chemical denaturation assays, as described in detail in Section 2.7. This approach allows us to explore stability changes over two different pathways on the energy landscape of the protein and gain a better understanding of the interplay between structure, stability, and function.

The thermal stability of CaM^{WT} and CaM mutants, in the presence and absence of Ca²⁺, was measured by CD spectroscopy and the data are shown in Figure 6. In the absence of Ca²⁺, all CaM proteins reveal a similar behavior unfolding in a cooperative manner, exhibiting a similar melting temperature (42.0°C–46.4°C). All recombinant CaM proteins appeared to be in a fully unfolded state at 80.0°C, where a stable CD signal was reached. In contrast, significant differences were observed for the thermal unfolding of CaM mutants in the presence of Ca²⁺. Under these conditions the CaM proteins showed a significant increase in thermal stability, with all proteins retaining some degree of secondary structure at very high temperatures (*T* > 90.0°C). This incomplete thermal

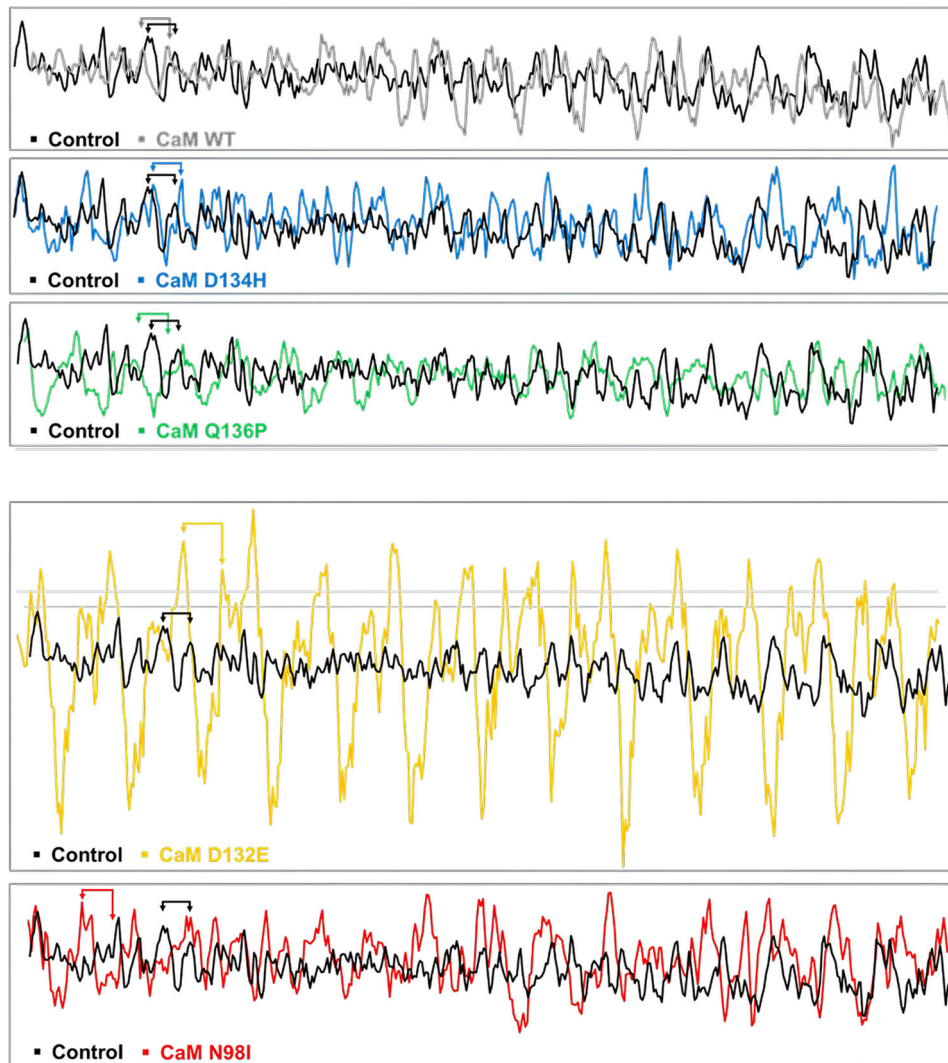


FIGURE 4 | Effect of expression of CaM variants on cardiac rhythm in zebrafish embryos. Cardiac rhythm activity was calculated from oscillations in the cardiac signal, with corresponding peaks and lows at regular intervals over time of a total of 6 s. Video recordings of high-speed acquisition of the blood flow (60 frames per second) were processed, and a selected area of the ventricle with circulating red blood cells was used to calculate the cardiac blood flow pulse. A representative flow profiles chart for the analysis provides a color-coded pulse over time (6 s) compiled from all recorded videos. Control, CaM^{WT}, CaM^{D134H}, and CaM^{Q136P}-microinjected zebrafish embryo groups exhibited the same pattern of oscillations at approximately 2.5 lows per second, while CaM^{N98I} and CaM^{D132E}-injected modeling resulted in arrhythmia evident by the altered oscillations and cardiac activity. CaM^{D132E} significantly altered the cardiac rhythm and oscillations at systole and diastole cycles. Representative charts at 72 h postfertilization (hpf). Video recordings of high-speed acquisition of the blood flow (60 frames per second) were processed, and a selected area of the ventricle with circulating red blood cells was used to calculate the cardiac pulse. A representative flow profiles chart for the analysis provides a color-coded pulse over time (6 s) ($n = 38, 28, 17, 41, 26,$ and 47 for control, CaM^{WT}, CaM^{N98I}, CaM^{D132E}, CaM^{D134H}, and CaM^{Q136P}, respectively).

transitions of all recombinant CaM proteins renders a more detailed analysis of the results very difficult and highly unreliable. However, for the temperature range of the CD measurements it is clear the the following order of thermal stability is observed: CaM^{WT} > CaM^{N98I} > CaM^{D132E} >> CaM^{D134H} – CaM^{Q136P}.

The chemical stability of the various CaM proteins reflects that observed for the thermal denaturation. In the absence of Ca²⁺, transition curves of CaM^{WT} and the four mutant proteins overlap reasonably well (Figure 7A; Supporting Information S1: Table 1). Fitting to a three state model (Equation 2) resulted in $D_{50,1}$ 0.9–1.8 M, and $D_{50,2}$ 2.0–2.5 M GuHCl; free energies ΔG_1 and ΔG_2 varied from –10 to –16 and –13 to –21 kJ/mol, respectively (Supporting Information S1: Table 1 and Supporting Information

S1: Figures 6–10). In the presence of Ca²⁺, $D_{50,1}$ increases to 1.3–2.2 M GuHCl with ΔG_1 –8 to –22 kJ/mol for CaM^{WT} and the CaM^{N98I} and CaM^{D132E} mutants (Figure 7B; Supporting Information S1: Table 1 and Supporting Information S1: Figures 11–15). For the CaM^{D134H} and CaM^{Q136P} mutant proteins, the native-to-intermediate transition could not be observed at 25°C, and thus data were fitted assuming a two-state intermediate-to-unfolded transition (Supporting Information S1: Figures 14 and 15). For all five recombinant CaM proteins $D_{50,2}$ values were very similar (3.4–3.9 M GuHCl) and ΔG_2 ca. –19 to –27 kJ/mol (Supporting Information S1: Table 1).

Interestingly, the thermal and chemical denaturation experiments suggest different order of stability for the wild-type and

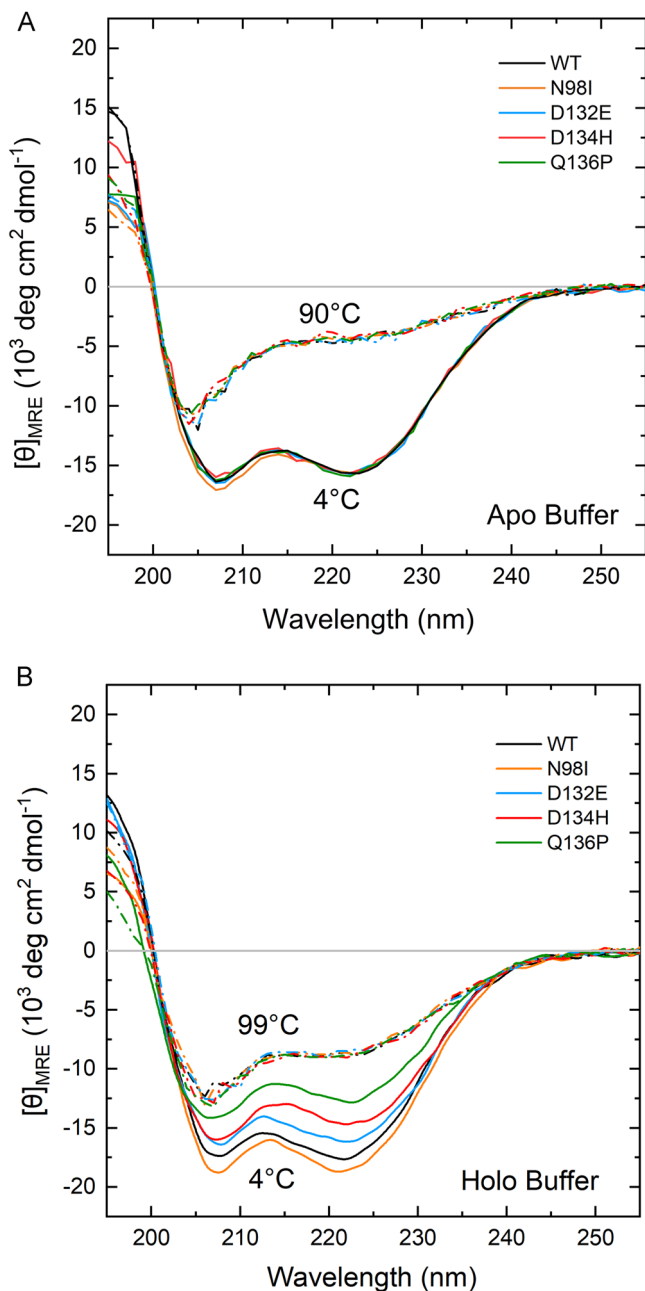


FIGURE 5 | Far-UV spectra of WT and mutant CaM proteins in the absence (A—apo-buffer) and presence of Ca^{2+} (B—holo-buffer). Solid lines correspond to spectra collected at low temperature (4°C), while dash-dot lines correspond to spectra collected at high temperatures ($\geq 90^\circ\text{C}$). CaM^{WT} , CaM^{N98I} , $\text{CaM}^{\text{D132E}}$, $\text{CaM}^{\text{D134H}}$, and $\text{CaM}^{\text{Q136P}}$ are shown as black, orange, cyan, red, and green lines, respectively.

mutant CaM proteins. This is not surprising as thermal and chemical denaturation transitions can follow different pathways on the energy landscape of the protein.

3.3 | D132E Mutation Results in the Most Deleterious Effect on the Ca^{2+} -Binding Properties of CaM C-Domain

Earlier studies [44, 45] demonstrated that domain-specific fluorescence changes in CaM at various Ca^{2+} concentrations

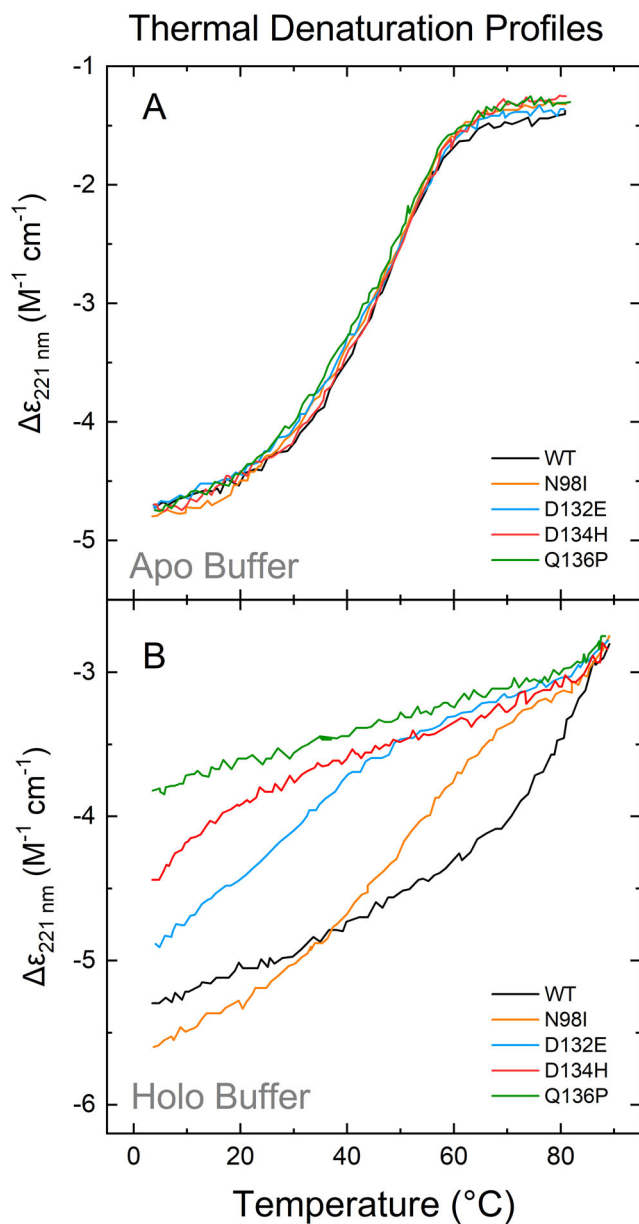


FIGURE 6 | Thermal denaturation profiles of recombinant purified CaM wild type and mutants. The 221 nm CD signal was monitored upon increasing temperature for CaM^{WT} (black line), CaM^{N98I} (orange line), $\text{CaM}^{\text{D132E}}$ (cyan line), $\text{CaM}^{\text{D134H}}$ (red line), and $\text{CaM}^{\text{Q136P}}$ (green line) in the presence of 1 mM EDTA (A) or 1 mM Ca^{2+} (B).

could be tracked by selective residue excitation. Using 277 nm as an excitation wavelength and 320 nm as a reference emission wavelength to monitor tyrosine fluorescence (C-terminal lobe emissions), we determined that both wild type and mutant CaM proteins exhibited an increase in fluorescence intensity as a function of free Ca^{2+} concentration (Supporting Information S1: Figure 16A). The situation is reverted when 250 nm is used as an excitation wavelength and 280 nm as a reference emission wavelength for selective phenylalanine excitation (N-terminal lobe emissions). In this case, the fluorescence intensity decreases with increasing Ca^{2+} concentration (Supporting Information S1: Figure 16B). Data sets from four separate experiments were fitted using global nonlinear regression to a model-independent two-site Adair function and the results are

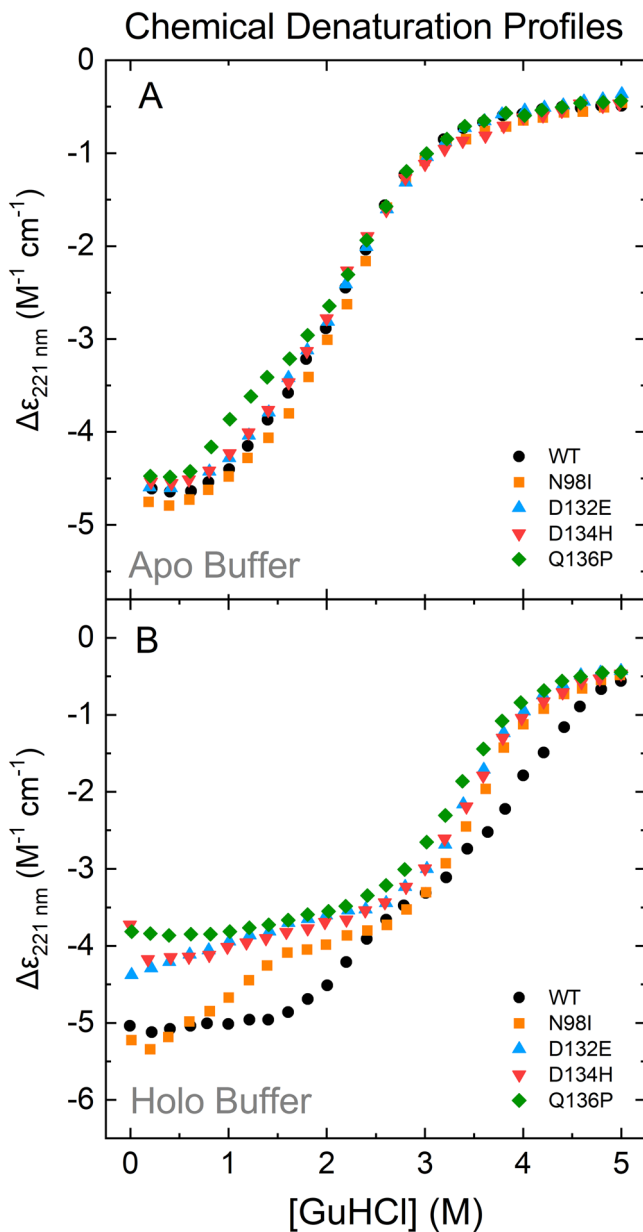


FIGURE 7 | Chemical denaturation profiles of recombinant purified CaM wild type and mutants. The 221 nm CD signal was monitored upon increasing chaotrope concentrations for CaM^{WT} (black circles), CaM^{N98I} (orange squares), CaM^{D132E} (cyan up triangles), CaM^{D134H} (red down triangles) and CaM^{Q136P} (green diamond) in the presence of 1 mM EDTA (A) or 1 mM Ca²⁺ (B).

summarized in Table 1 and Supporting Information S1: Figures 17 and 18.

For the wild-type, C-terminal lobe binding sites have an apparent K_d almost three times higher than that of the N-terminal binding sites (2.97 and 8.08 μ M, respectively, Table 1). The free energy change that accompanies the binding of two Ca²⁺ at the C-terminal binding sites was found to be -63.1 kJ/mol (ΔG_2) with a cooperative free energy change of -9.8 kJ/mol (ΔG_c), while the corresponding values for the N-domain binding sites were -58.2 and -4.3 kJ/mol, respectively. These calculations are in good agreement with earlier studies under the same experimental conditions [11].

N-Domain binding sites show only small differences between wild-type and mutant CaM proteins in terms of Ca²⁺ binding affinity (Table 1). This is not surprising considering that all the mutations in this study are distally located in the C-terminal lobe of the protein. In contrast, for the C-terminal lobe binding sites, all CaM mutants showed reduced Ca²⁺ affinities compared to CaM wild-type (Table 1). The most moderate effect is that of CaM^{Q136P}, with a dissociation constant of 19 μ M, almost seven times higher than that of the wild type. CaM^{N98I} and CaM^{D134H} had slightly higher dissociation constants (23 and 30 μ M respectively), while the most severe impact is on D132E, as we found that CaM^{D132E} variant exhibited 14 times lower Ca²⁺ affinity compared to wild-type CaM. Thermodynamic analysis of the free energy changes upon Ca²⁺ binding to the C-domain binding sites reveals an interesting picture (Table 1, Supporting Information S1: Figure 18). The free energy change for the CaM variants is similar to that of the wild type when only one binding site is occupied (ranging from 2.6 to 1.3 kJ/mol less, ΔG_1), whereas the total free energy change for binding to both C-terminal lobe binding sites is significantly reduced (ranging from 13.0 to 9.2 kJ/mol less, ΔG_2). This effect can be associated with the change of cooperativity between the two binding sites as revealed by the lower limit estimates for the free energy change attributed to cooperativity (ΔG_c). For the CaM^{Q136P}, CaM^{N98I}, and CaM^{D134H} mutants, ΔG_c is 51%, 46%, and 37% of the wild type, respectively, while for D132E is negligible, signifying absence of cooperativity between the two C-terminal lobe binding sites. Moreover, it is worth noting that our findings regarding the Ca²⁺-binding affinities for the C-domains of these CaM mutants are consistent and in good agreement with another study that previously reported the dissociation constants of these mutants [11] (Supporting Information S1: Table 2).

An ensemble of model structures was created for each CaM mutant with MOE 2022.02 software using PDB entry 1CLL as template. The generated mutant models were compared to the wild-type structure to get an insight on the C-terminal lobe binding sites structural alterations. Based on our models, CaM^{Q136P}, CaM^{N98I}, and CaM^{D134H} mutants (Figure 8A,C,D) show no significant changes in binding pocket shape with the exception of the altered residues themselves. It seems even these minute local structural changes in the binding pocket can measurably affect the flexibility and thus the cooperativity of the CaM binding sites. In contrast, for CaM^{D132E} (Figure 8B), there is substantial reorientation of key-placed residues inside the binding pocket, that eventually leads to complete loss of cooperativity as per our Ca²⁺ binding experiments suggested above. In addition, generated models for the apo-CaM binding pockets (Supporting Information S1: Figure 19) showed very small changes in the structural organization of the EF-hand motifs.

4 | Discussion

Genetic testing identified pathogenic CaM variants with variable spectrum of clinical presentations. Since 2012, when the first two missense CaM variants (N54I and N98S) were identified in individuals with CPVT-like symptoms, more than 30 missense CaM variants have been reported [1, 10–14, 46–48].

TABLE 1 | Summary of biophysical measurements for CaM wild type and mutants. Dissociation constants and free energy changes of Ca^{2+} binding to recombinant CaM protein C- (exc: 277 nm, ems: 320 nm) and N-domain sites (exc: 250 nm, ems: 280 nm) at 25°C, resolved from fitting of a model-independent two-site Adair to function the experimental data.

	Apparent dissociation constant (K_d) μM	ΔG_1 kJ/mol	ΔG_2 kJ/mol	ΔG_c kJ/mol
WT				
C-Domain	2.97 ± 0.03	-28.4 ± 0.2	-63.1 ± 0.1	-9.8 ± 0.3
N-Domain	8.08 ± 0.09	-28.7 ± 0.2	-58.2 ± 0.1	-4.3 ± 0.3
D132E				
C-Domain	41.55 ± 0.15	-27.1 ± 0.2	-50.1 ± 0.2	0.6 ± 0.4
N-Domain	7.09 ± 0.23	-29.8 ± 0.3	-58.8 ± 0.2	-2.7 ± 0.6
D134H				
C-Domain	29.56 ± 0.08	-25.8 ± 0.3	-51.7 ± 0.2	-3.6 ± 0.5
N-Domain	7.64 ± 0.19	-29.7 ± 0.2	-58.5 ± 0.2	-2.5 ± 0.4
Q136P				
C-Domain	19.03 ± 0.07	-26.2 ± 0.4	-53.9 ± 0.2	-5.0 ± 0.8
N-Domain	7.24 ± 0.17	-24.9 ± 0.9	-58.7 ± 0.2	-12.3 ± 1.9
N98I				
C-Domain	23.40 ± 0.08	-25.9 ± 0.4	-52.9 ± 0.2	-4.5 ± 0.8
N-Domain	7.15 ± 0.12	-25.8 ± 0.6	-58.8 ± 0.1	-10.6 ± 1.2

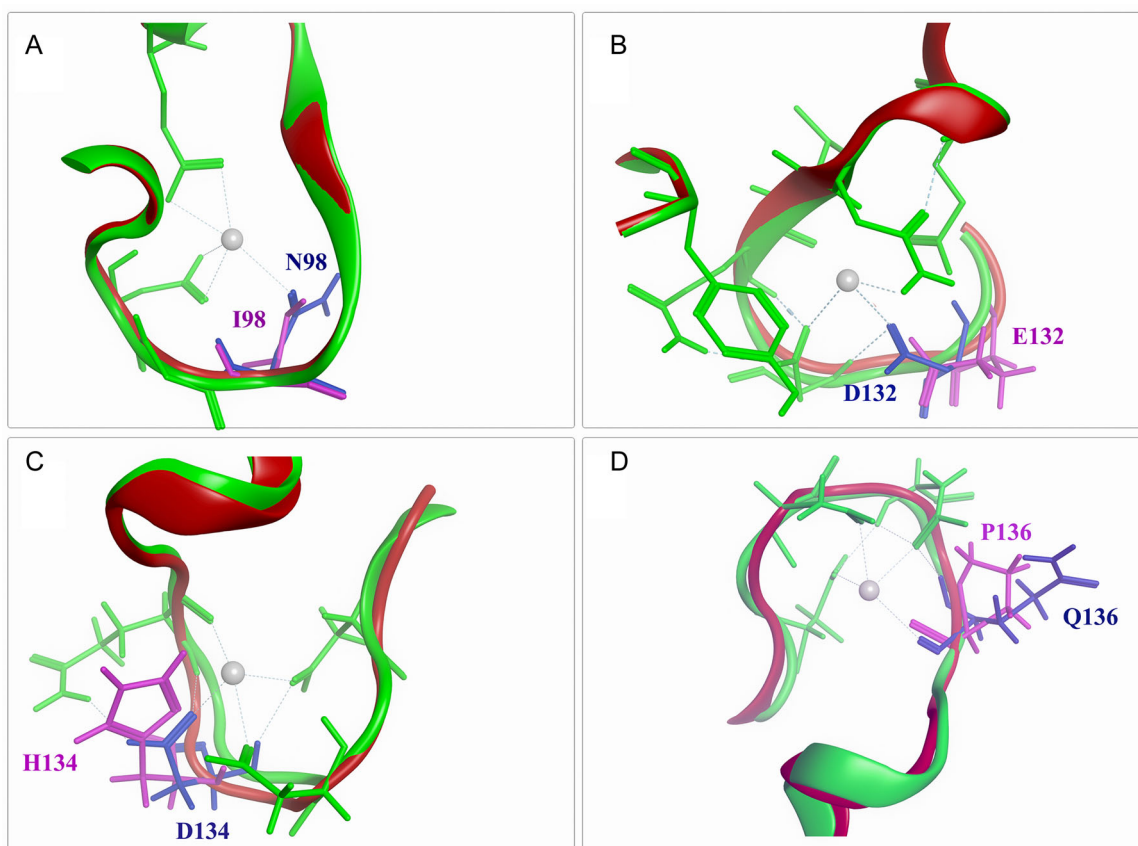


FIGURE 8 | Schematic models of the CaM mutants. Overlap of wild type (green) and mutant (red) energy-minimized models of wild type and (A) N98I, (B) D132E, (C) D134H, and (D) Q136P CaM binding sites with key residues shown as sticks. Figure is based on PDB entry 1CLL. Ca^{2+} ions are shown as gray spheres. Mutations are shown with magenta, while the corresponding wild-type residue is shown with blue.

Interestingly, these missense mutations are predominantly located in the C-terminal lobe of CaM, affecting residues involved in Ca²⁺ binding and thus leading to reduction of CaM Ca²⁺-binding affinity. However, the identified CaM E46K and N54I N-terminal lobe mutations do not seem to affect Ca²⁺-binding, since they are not in close proximity to the Ca²⁺-binding pockets [20, 49, 50]. In the present study, we selected four missense CaM mutations located in the EF hand domains III and IV of the C-terminal lobe that have not yet been characterized extensively. All four mutations were found to be located in the *CALM2* gene. N98I was identified in a 17 month-old boy from England that was diagnosed with LQTS. D132E was discovered in a 29 year-old woman from Germany that was diagnosed with neonatal LQTS and later in her life with CPVT. D134H was identified in a 6 year-old girl from Japan that was diagnosed with LQTS. Finally, Q136P was found in an 8 year-old girl from Morocco that died during exercise even though she was taking β -blockers to treat her LQTS and CPVT symptoms [11].

We initially synthesized cRNA corresponding to human CaM wild-type and its aforementioned mutants and we microinjected it into zebrafish embryos, to investigate the *in vivo* effects of the expression of these CaM mutants on zebrafish cardiac structure and function. All zebrafish larvae exhibited a well-developed ventricle, except the groups that expressed the CaM^{N98I} and CaM^{D134H} mutants, which revealed a negative structural ventricle chamber shape effect. This is not the first time that we observed a morphological abnormality in the ventricle chamber of the zebrafish heart. In a previous study, we have reported a similar heart abnormality when zebrafish embryos were microinjected with cRNA corresponding to human CaM^{E105A} mutant, which was identified in a 6 year-old boy diagnosed with LQTS [14, 24]. Expression of human CaM^{WT} into zebrafish embryos resulted in an average heart rate of 145.7 bpm with no statistically significant difference from the control group (150.9 bpm). In contrast, expression of human CaM^{D132E} and CaM^{D134H} variants into zebrafish resulted in a significant reduction of the zebrafish heart rate, mimicking a severe form of human bradycardia. Interestingly, this is in agreement with the clinical phenotype of the patients identified to carry these mutations, who presented with fetal and perinatal bradycardia [11]. Moreover, Berchtold et al. observed a similar reduction of zebrafish heart rate when they microinjected cRNA corresponding to human CaM^{D130G} in zebrafish embryos [51]. The CaM^{D130G} has been previously identified in individuals diagnosed with LQTS [9, 48, 52]. Regarding CaM^{N98I}, we observed a trend towards lower heart rate for this variant, albeit not statistically significant (Figure 3). At the same location of CaM protein, another mutant, CaM^{N98S}, was identified in individuals with LQTS and CPVT symptoms. Interestingly, expression of human CaM^{N98S} into zebrafish embryos resulted in an increased heart rate that is related to β adrenergic stimulation [53]. Expression of CaM^{Q136P} in zebrafish resulted in an increased heart rate of 157.4 bpm, mimicking human ventricular tachycardia when compared to both control and CaM^{WT} heart rates (Figure 3).

Analysis of their cardiac ventricular rhythm revealed that CaM^{D132E} and CaM^{N98I} microinjected zebrafish groups displayed an irregular pattern of heart beating and increased

amplitude of the cardiac rhythm in comparison to the cardiac activity percentage mean of the control, CaM^{WT}, CaM^{D134H}, and CaM^{Q136P} groups (Figure 4), demonstrating that CaM^{D132E} and CaM^{N98I} mutants result in an increased arrhythmic potential in the zebrafish model. Sondergaard et al. also observed that microinjection of CaM^{N54I} and CaM^{N98S} in zebrafish embryos produced an increased arrhythmic potential, since the hearts of CaM^{N54I} and CaM^{N98S}-microinjected zebrafish displayed a shorter diastolic interval compared to the hearts of CaM^{WT}-microinjected zebrafish embryos [53]. Moreover, Berchtold et al. noticed in a subpopulation of CaM^{D130G} zebrafish embryos that the atrium beats twice per ventricular contraction suggesting an increased arrhythmic potential in these zebrafish as well [51].

The thermal stability of CaM^{WT} and CaM mutant proteins was measured in the absence of Ca²⁺ and the melting temperatures of CaM^{WT} and all mutants were found to be rather similar. However, in the presence of Ca²⁺, we observed significant differences in thermostability, following the order CaM^{WT} > CaM^{N98I} > CaM^{D132E} >> CaM^{D134H} - CaM^{Q136P}. It was well noticed that in the presence of Ca²⁺, D134H and Q136P mutations appear to have the most significant negative effect on CaM stability, with our thermal unfolding findings being in overall agreement with the chemical denaturation data.

Regarding the affinity for Ca²⁺, all CaM mutants showed reduced C-lobe Ca²⁺ affinities compared to CaM wild-type (Table 1, Supporting Information S1: Figure 16A). While CaM^{Q136P} had a dissociation constant almost seven times higher than that of the wild-type, CaM^{N98I} and CaM^{D134H} had only a slightly higher dissociation constant. The most severe impact is in the D132E mutation; as we found that CaM^{D132E} mutant exhibited around 14 times lower Ca²⁺ affinity compared to wild-type CaM. This is in good agreement with our structural modeling, where D132E mutation appeared to have the most severe impact on the Ca²⁺ binding site. Moreover, all mutations located in the C-terminal lobe of CaM that have been studied up to date have shown reduced Ca²⁺ affinity [20]. We previously showed that the N-lobe CaM N54I mutation has no effect on the Ca²⁺-binding affinity of CaM [20, 24, 54]. A well-known feature of CaM is the high cooperativity of Ca²⁺ binding within its individual lobes. It is generally accepted that a high level of positive cooperativity exists between EF1 and EF2 in the lower affinity N-lobe, and EF3 and EF4 in the higher affinity C-lobe. This applies to the mutations we study here since the free energy change for the CaM variants is similar to that of the wild-type when only one binding site is occupied, while the total free energy change for binding to both C-terminal lobe binding sites is significantly reduced. This effect is connected to the loss of cooperativity between the two binding sites as revealed by the lower limit estimates for the free energy change due to cooperativity (ΔG_c). For the CaM^{Q136P}, CaM^{N98I}, and CaM^{D134H} mutants ΔG_c is 51%, 46%, and 37% of the wild-type, respectively, whereas for CaM^{D132E} it is negligible (Table 1), consistent with a complete loss of cooperativity between the two Ca²⁺ binding sites of the C-terminal lobe.

Overlap of energy-minimizing models of CaM^{Q136P}, CaM^{N98I}, and CaM^{D134H} mutants with CaM^{WT} model (Figure 8A,C,D) show no significant changes in binding pocket shape with the exception of the altered residues themselves. In contrast, for

CaM^{D132E} (Figure 8B), there is substantial reorientation of key-placed residues inside the binding pocket, that eventually leads to complete loss of cooperativity. Aspartate has a shorter side chain than the very similar glutamate residue, meaning that it is slightly more rigid within protein structures and gives it a slightly stronger preference to be involved in protein active sites. In the case of CaM^{D132E}, substitution of the aspartate residue by the bulkier glutamate probably leads to a reorientation of key-placed residues inside the binding pocket that eventually leads to complete loss of cooperativity.

In a recent study, where we characterized the interaction of these four CaM mutants with RyR2, we found that all mutants displayed a dramatically reduced RyR2 interaction as well as defective modulation of [³H]ryanodine binding to RyR2 [25]. Moreover, our isothermal titration experiments investigating the interaction of these CaM mutants with two human RyR2 CaM-binding regions (3584–3602aa and 4255–4271aa), that we proposed might contribute to a putative intra-subunit CaM-binding pocket, showed disparate binding properties suggesting that differential mechanisms might contribute to reduced CaM-RyR2 association [25, 55]. Furthermore, another study, which performed Ca²⁺-dependent titration experiments of a fluorescently labeled peptide corresponding to the RyR2 CaM-binding region 3581–3611aa, revealed that the same arrhythmogenic CaM mutants conferred a decreased affinity for this peptide, altering the Ca²⁺-dependency of CaM-RyR2 peptide binding [56]. More importantly, the authors showed that these CaM mutations lead to a diminished CaM-dependent inhibition of Ca²⁺ release and increased store-overload induced Ca²⁺ release in HEK cells. In addition, all four CaM mutants were not only unable to inhibit, but promoted RyR2-mediated Ca²⁺ release in permeabilized HEK293 cells [56]. CaM-RyR2 interaction is highly dependent on the cytoplasmic calcium concentrations. Loss of Ca²⁺-binding affinity can result in a reduced/abolished interaction and thus regulation of RyR2, which can provide one potential molecular mechanism for the arrhythmogenesis observed in the patients carrying the aforementioned CaM mutations.

Over the last couple of years, the fact that numerous genetic and clinical studies reported several pathogenic CaM mutations associated with life-threatening arrhythmogenic presentations, has led to a new, distinct clinical entity termed as calmodulinopathy, which can be caused by mutations in any of the three *CALM* genes. Congenital LQTS and CPVT are the two most typical clinical manifestations of calmodulinopathy, increasing the risk of repeated syncope, lethal arrhythmic events and sudden cardiac death, particularly in young individuals [19]. Interestingly, the identification of CaM mutations, such as the D132E and Q136P associated with a clinical presentation of mixed LQTS and CPVT phenotypes is particularly intriguing since it emphasizes the potential that particular clinical presentation(s) are caused by various factors, including the amino acid change, genetic/protein sequence location, the total amount of the mutant protein expressed and its ratio to the wild-type, as well as the impact of the mutation on the Ca²⁺-binding affinity of CaM, as this latter parameter can directly affect vital interactions of CaM with multiple proteins/ion channels in the heart, including Ca_v1.2 and RyR2 [25]. The disparate impact of the CaM mutations that we investigated in this study on zebrafish cardiac function strongly supports this

notion. It is clear that further investigation is required to elucidate the complex mechanism(s) that underly how various CaM mutations lead to arrhythmogenic cardiac disease and sudden cardiac death. Moreover, due to the multifactorial nature of the disease, and based on the fact that limited information on the clinical efficacy of existing therapies is currently available, systematic genetic screening and clinical evaluation of the patients, along with functional validation studies, is necessary until the development of future gene correction approaches is achieved through precision medicine.

Author Contributions

Michail Nomikos and F. Anthony Lai: conceptualization. **Sahar I. Da'as, Angelos Thanassoulas, Bared Safieh-Garabedian, Gheyath K. Nasrallah, George Nounesis, F. Anthony Lai, and Michail Nomikos:** methodology. **Sahar I. Da'as, Angelos Thanassoulas, and Michail Nomikos:** formal analysis. **Sahar I. Da'as, Angelos Thanassoulas, Gheyath K. Nasrallah, George Nounesis, F. Anthony Lai, and Michail Nomikos:** validation. **Sahar I. Da'as, Angelos Thanassoulas, Brian L. Calver, Alaaeldin Saleh, Doua Abdelrahman, Iris Kontogianni, and Michail Nomikos:** investigation. **Gheyath K. Nasrallah and Michail Nomikos:** resources. **Sahar I. Da'as, Angelos Thanassoulas, Waseem Hasan, Gheyath K. Nasrallah, and Michail Nomikos:** data curation. **Michail Nomikos:** writing—original draft preparation. **Sahar I. Da'as, Angelos Thanassoulas, Brian L. Calver, Alaaeldin Saleh, Waseem Hasan, Bared Safieh-Garabedian, Gheyath K. Nasrallah, George Nounesis, F. Anthony Lai, and Michail Nomikos:** writing—review and editing. **George Nounesis, F. Anthony Lai, and Michail Nomikos:** supervision. All authors have read and agreed to the published version of the manuscript.

Acknowledgments

We would like to thank Dr. Konrad Beck for his assistance with the CD experiments. We are also grateful to Xuexun Fang (Laboratory of Molecular Enzymology and Enzyme Engineering of the Ministry of Education, Jilin University, China) for providing the pHSIE vector. Michail Nomikos was supported by QU Internal Grants “QUCG-CMED-19/20-2” and “QUCG-CMED-22/23-514”. Gheyath K. Nasrallah would like to acknowledge funds from UREP grant # (UREP26-097-3-040) and HSREP02-1125-190004 from Qatar National Research Fund (a member of Qatar Foundation). The statements made herein are solely the responsibility of the author. The open access publication of this article was funded by Qatar National Library.

Conflicts of Interest

The authors declare no conflicts of interest.

Data Availability Statement

The data that support the findings of this study are available from the corresponding author upon reasonable request.

References

1. J. W. Hussey, W. B. Limpitikul, and I. E. Dick, “Calmodulin Mutations in Human Disease,” *Channels* 17 (2023): 2165278.
2. M. R. Tadross, I. E. Dick, and D. T. Yue, “Mechanism of Local and Global Ca²⁺ Sensing by Calmodulin in Complex with a Ca²⁺ Channel,” *Cell* 133 (2008): 1228–1240.
3. A. Villalobo, “The Multifunctional Role of Phospho-Calmodulin in Pathophysiological Processes,” *Biochemical Journal* 475 (2018): 4011–4023.

4. A. Villalobo, H. Ishida, H. J. Vogel, and M. W. Berchtold, "Calmodulin as a Protein Linker and a Regulator of Adaptor/Scaffold Proteins," *Biochimica et Biophysica Acta (BBA)—Molecular Cell Research* 1865 (2018): 507–521.
5. M. Zhang, C. Abrams, L. Wang, et al., "Structural Basis for Calmodulin as a Dynamic Calcium Sensor," *Structure* 20 (2012): 911–923.
6. S. Linse, A. Helmersson, and S. Forsén, "Calcium Binding to Calmodulin and Its Globular Domains," *Journal of Biological Chemistry* 266 (1991): 8050–8054.
7. M. W. Berchtold, R. Egli, J. A. Rhyner, H. Hameister, and E. E. Strehler, "Localization of the Human Bona Fide Calmodulin Genes CALM1, CALM2, and CALM3 to Chromosomes 14q24-q31, 2p21.1-p21.3, and 19q13.2-q13.3," *Genomics* 16 (1993): 461–465.
8. R. Fischer, M. Koller, M. Flura, et al., "Multiple Divergent mRNAs Code for a Single Human Calmodulin," *Journal of Biological Chemistry* 263 (1988): 17055–17062.
9. L. Crotti, C. N. Johnson, E. Graf, et al., "Calmodulin Mutations Associated With Recurrent Cardiac Arrest in Infants," *Circulation* 127 (2013): 1009–1017.
10. J. Gao, T. Makiyama, Y. Yamamoto, et al., "Novel Calmodulin Variant p.E46K Associated With Severe Catecholaminergic Polymorphic Ventricular Tachycardia Produces Robust Arrhythmogenicity in Human Induced Pluripotent Stem Cell-Derived Cardiomyocytes," *Circulation: Arrhythmia and Electrophysiology* 16 (2023): e011387.
11. N. Makita, N. Yagihara, L. Crotti, et al., "Novel Calmodulin Mutations Associated With Congenital Arrhythmia Susceptibility," *Circulation: Cardiovascular Genetics* 7 (2014): 466–474.
12. R. F. Marsman, J. Barc, L. Beekman, et al., "A mutation in CALM1 Encoding Calmodulin in Familial Idiopathic Ventricular Fibrillation in Childhood and Adolescence," *Journal of the American College of Cardiology* 63 (2014): 259–266.
13. M. Nyegaard, M. T. Overgaard, M. T. Søndergaard, et al., "Mutations in Calmodulin Cause Ventricular Tachycardia and Sudden Cardiac Death," *The American Journal of Human Genetics* 91 (2012): 703–712.
14. K. Takahashi, T. Ishikawa, N. Makita, K. Takefuta, T. Nabeshima, and M. Nakayashiro, "A Novel De Novo Calmodulin Mutation in a 6-Year-Old Boy Who Experienced an Aborted Cardiac Arrest," *HeartRhythm Case Reports* 3 (2017): 69–72.
15. N. Gomez-Hurtado, N. J. Boczek, D. O. Kryshal, et al., "Novel CPVT-Associated Calmodulin Mutation in CALM3 (CALM3-A103V) Activates Arrhythmogenic Ca Waves and Sparks," *Circulation: Arrhythmia and Electrophysiology* 9 (2016): e004161.
16. H. S. Hwang, F. R. Nitu, Y. Yang, et al., "Divergent Regulation of Ryanodine Receptor 2 Calcium Release Channels by Arrhythmogenic Human Calmodulin Missense Mutants," *Circulation Research* 114 (2014): 1114–1124.
17. W. B. Limpitikul, I. E. Dick, R. Joshi-Mukherjee, M. T. Overgaard, A. L. George Jr., and D. T. Yue, "Calmodulin Mutations Associated With Long Qt Syndrome Prevent Inactivation Of Cardiac L-Type Ca(2+) Currents and Promote Proarrhythmic Behavior in Ventricular Myocytes," *Journal of Molecular and Cellular Cardiology* 74 (2014): 115–124.
18. M. Nomikos, A. Thanassoulas, K. Beck, et al., "Altered RyR2 Regulation by the Calmodulin F90L Mutation Associated With Idiopathic Ventricular Fibrillation and Early Sudden Cardiac Death," *FEBS Letters* 588 (2014): 2898–2902.
19. W. C. Tsai, P. S. Chen, and M. Rubart, "Calmodulinopathy in Inherited Arrhythmia Syndromes," *Tzu Chi Medical Journal* 33 (2021): 339–344.
20. V. Vassilakopoulou, B. L. Calver, A. Thanassoulas, et al., "Distinctive Malfunctions of Calmodulin Mutations Associated With Heart RyR2-Mediated Arrhythmic Disease," *Biochimica et Biophysica Acta (BBA)—General Subjects* 1850 (2015): 2168–2176.
21. D. M. Balshaw, L. Xu, N. Yamaguchi, D. A. Pasek, and G. Meissner, "Calmodulin Binding And Inhibition of Cardiac Muscle Calcium Release Channel (Ryanodine Receptor)," *Journal of Biological Chemistry* 276 (2001): 20144–20153.
22. N. Yamaguchi, N. Takahashi, L. Xu, O. Smithies, and G. Meissner, "Early Cardiac Hypertrophy in Mice With Impaired Calmodulin Regulation of Cardiac Muscle Ca²⁺ Release Channel," *Journal of Clinical Investigation* 117 (2007): 1344–1353.
23. Y. Yang, T. Guo, T. Oda, et al., "Cardiac Myocyte Z-Line Calmodulin is Mainly RyR2-Bound, and Reduction is Arrhythmogenic and Occurs in Heart Failure," *Circulation Research* 114 (2014): 295–306.
24. S. I. Da'as, A. Thanassoulas, B. L. Calver, et al., "Arrhythmogenic Calmodulin E105A Mutation Alters Cardiac RyR2 Regulation Leading to Cardiac Dysfunction in Zebrafish," *Annals of the New York Academy of Sciences* 1448 (2019): 19–29.
25. A. Thanassoulas, V. Vassilakopoulou, B. L. Calver, et al., "Life-Threatening Arrhythmogenic CaM Mutations Disrupt CaM Binding to a Distinct RyR2 CaM-Binding Pocket," *Biochimica et Biophysica Acta (BBA)—General Subjects* 1867 (2023): 130313.
26. M. Brohus, M. T. Søndergaard, S. R. Wayne Chen, F. van Petegem, and M. T. Overgaard, "Ca(2+)-Dependent Calmodulin Binding to Cardiac Ryanodine Receptor (RyR2) Calmodulin-Binding Domains," *Biochemical Journal* 476 (2019): 193–209.
27. K. Lau, M. M. Y. Chan, and F. Van Petegem, "Lobe-Specific Calmodulin Binding to Different Ryanodine Receptor Isoforms," *Biochemistry* 53 (2014): 932–946.
28. C. B. Klee, "Conformational Transition Accompanying the Binding of Ca²⁺ to the Protein Activator of 3',5'-cyclic Adenosine Monophosphate Phosphodiesterase," *Biochemistry* 16 (1977): 1017–1024.
29. Y. Nozaki, "The Preparation of Guanidine Hydrochloride," *Methods in Enzymology* 26 (1972): 43–50.
30. L. Masino, S. R. Martin, and P. M. Bayley, "Ligand Binding and Thermodynamic Stability of a Multidomain Protein, Calmodulin," *Protein Science* 9 (2000): 1519–1529.
31. Q. Wang, K. C. Liang, A. Czader, M. N. Waxham, and M. S. Cheung, "The Effect of Macromolecular Crowding, Ionic Strength and Calcium Binding on Calmodulin Dynamics," *PLoS Computational Biology* 7 (2011): e1002114.
32. G. K. Ackers, M. A. Shea, and F. R. Smith, "Free Energy Coupling Within Macromolecules," *Journal of Molecular Biology* 170 (1983): 223–242.
33. S. Pedigo and M. A. Shea, "Discontinuous Equilibrium Titrations of Cooperative Calcium Binding to Calmodulin Monitored by 1-D 1H-Nuclear Magnetic Resonance Spectroscopy," *Biochemistry* 34 (1995): 10676–10689.
34. S. Pedigo and M. A. Shea, "Quantitative Endoproteinase GluC Footprinting of Cooperative Ca²⁺ Binding to Calmodulin: Proteolytic Susceptibility of E31 and E87 Indicates Interdomain Interactions," *Biochemistry* 34 (1995): 1179–1196.
35. S. I. Da'as, K. Fakhro, A. Thanassoulas, et al., "Hypertrophic Cardiomyopathy-linked Variants of Cardiac Myosin-binding Protein C3 Display Altered Molecular Properties and Actin Interaction," *Biochemical Journal* 475 (2018): 3933–3948.
36. S. I. Da'as, W. Hasan, R. Salem, et al., "Transcriptome Profile Identifies Actin as an Essential Regulator of Cardiac Myosin Binding Protein C3 Hypertrophic Cardiomyopathy in a Zebrafish Model," *International Journal of Molecular Sciences* 23 (2022): 8840.
37. S. I. Da'as, H. C. Yalcin, G. K. Nasrallah, et al., "Functional Characterization of Human Myosin-Binding Protein C3 Variants

- Associated With Hypertrophic Cardiomyopathy Reveals Exon-Specific Cardiac Phenotypes in Zebrafish Model,” *Journal of Cellular Physiology* 235 (2020): 7870–7888.
38. F. M. Benslimane, Z. Z. Zakaria, S. Shurbaji, et al., “Cardiac Function and Blood Flow Hemodynamics Assessment of Zebrafish (*Danio rerio*) Using High-Speed Video Microscopy,” *Micron* 136 (2020): 102876.
39. B. Pelster and W. W. Burggren, “Disruption of Hemoglobin Oxygen Transport Does Not Impact Oxygen-dependent Physiological Processes in Developing Embryos of Zebra Fish (*Danio rerio*),” *Circulation Research* 79 (1996): 358–362.
40. L. McCormick, K. Wadmore, A. Milburn, et al., “Long QT Syndrome-Associated Calmodulin Variants Disrupt the Activity of the Slowly Activating Delayed Rectifier Potassium Channel,” *The Journal of Physiology* 601 (2023): 3739–3764.
41. G. Dal Cortivo, C. G. Barracchia, V. Marino, M. D’Onofrio, and D. Dell’Orco, “Alterations in Calmodulin-Cardiac Ryanodine Receptor Molecular Recognition in Congenital Arrhythmias,” *Cellular and Molecular Life Sciences* 79 (2022): 127.
42. K. Wang, M. Brohus, C. Holt, M. T. Overgaard, R. Wimmer, and F. Van Petegem, “Arrhythmia Mutations in Calmodulin Can Disrupt Cooperativity of Ca(2+) Binding and Cause Misfolding,” *The Journal of Physiology* 598 (2020): 1169–1186.
43. G. Dal Cortivo, V. Marino, S. Bianconi, and D. Dell’Orco, “Calmodulin Variants Associated With Congenital Arrhythmia Impair Selectivity for Ryanodine Receptors,” *Front Mol Biosci* 9 (2022): 1100992.
44. W. S. VanScyoc and M. A. Shea, “Phenylalanine Fluorescence Studies of Calcium Binding to N-Domain Fragments of Paramecium Calmodulin Mutants Show Increased Calcium Affinity Correlates With Increased Disorder,” *Protein Science* 10 (2001): 1758–1768.
45. W. S. VanScyoc, B. R. Sorensen, E. Rusinova, W. R. Laws, J. B. A. Ross, and M. A. Shea, “Calcium Binding to Calmodulin Mutants Monitored by Domain-Specific Intrinsic Phenylalanine and Tyrosine Fluorescence,” *Biophysical Journal* 83 (2002): 2767–2780.
46. M. A. Chaix, T. T. Koopmann, P. Goyette, et al., “Novel CALM3 Mutations in Pediatric Long QT Syndrome Patients Support a CALM3-Specific Calmodulinopathy,” *HeartRhythm Case Reports* 2 (2016): 250–254.
47. L. Crotti, C. Spazzolini, D. J. Tester, et al., “Calmodulin Mutations and Life-threatening Cardiac Arrhythmias: Insights From the International Calmodulinopathy Registry,” *European Heart Journal* 40 (2019): 2964–2975.
48. G. J. Reed, N. J. Boczek, S. P. Etheridge, and M. J. Ackerman, “CALM3 Mutation Associated With Long QT Syndrome,” *Heart Rhythm* 12 (2015): 419–422.
49. H. H. Jensen, M. Brohus, M. Nyegaard, and M. T. Overgaard, “Human Calmodulin Mutations,” *Frontiers in Molecular Neuroscience* 11 (2018): 396.
50. J. Urrutia, A. Aguado, A. Muguruza-Montero, et al., “The Crossroad of Ion Channels and Calmodulin in Disease,” *International Journal of Molecular Sciences* 20 (2019): 400.
51. M. W. Berchtold, T. Zacharias, K. Kulej, et al., “The Arrhythmogenic Calmodulin Mutation D129G Dysregulates Cell Growth, Calmodulin-dependent Kinase II Activity, and Cardiac Function in Zebrafish,” *Journal of Biological Chemistry* 291 (2016): 26636–26646.
52. N. J. Boczek, N. Gomez-Hurtado, D. Ye, et al., “Spectrum and Prevalence of CALM1-, CALM2-, and CALM3-Encoded Calmodulin Variants in Long QT Syndrome and Functional Characterization of a Novel Long QT Syndrome-Associated Calmodulin Missense Variant, E141G,” *Circulation: Cardiovascular Genetics* 9 (2016): 136–146.
53. M. T. Søndergaard, A. B. Sorensen, L. L. Skov, et al., “Calmodulin Mutations Causing Catecholaminergic Polymorphic Ventricular Tachycardia Confer Opposing Functional and Biophysical Molecular Changes,” *The FEBS Journal* 282 (2015): 803–816.
54. J. Su, Q. Gao, L. Yu, et al., “The LQT-Associated Calmodulin Mutant E141G Induces Disturbed Ca(2+)-Dependent Binding and a Flickering Gating Mode of the Ca(V)1.2 Channel,” *American Journal of Physiology-Cell Physiology* 318 (2020): C991–C1004.
55. A. Thanassoulas, M. Theodoridou, and L. Barrak, et al., “Arrhythmia-Associated Calmodulin E105A Mutation Alters the Binding Affinity of CaM to a Ryanodine Receptor 2 CaM-Binding Pocket,” *International Journal of Molecular Science* 24 (2023): 15630.
56. M. T. Søndergaard, Y. Liu, M. Brohus, et al., “Diminished Inhibition and Facilitated Activation of RyR2-Mediated Ca(2+) Release is a Common Defect of Arrhythmogenic Calmodulin Mutations,” *The FEBS Journal* 286 (2019): 4554–4578.

Supporting Information

Additional supporting information can be found online in the Supporting Information section.